Technical article

Optimization of induction motor with pole-changing winding by finite element models

Abstract — For induction drives that are operated at two speeds the approved Dahlander technology with pole changeable coils in the stator of the motor can be applied. Being operated at constant supply frequency the motor with Dahlander coils can be driven at a speed ratio of 2:1 without using a frequency converter. The advantages are the simplicity and the robustness of the machine as well as the saving of weight and installation space due to the omitted power electronic circuits, although the motor and its pole changeable coils have to be designed with particular care. Especially under given design constrains the classical design procedure shows it shortcomings and numerical techniques, such as the finite element method have to be applied to come to a design that meets the requirements.

While the Dahlander winding for single frequency operation has often been made subject of discussion, this paper presents the approach of an induction machine with pole-changing coils operating on mains supply with variable frequency for aircraft application. The two-dimensional finite element method is used to optimize the mean airgap flux density for both number of pole-pairs. Measurements on a prototype of the machine show that the required performance for the use as a pump drive is achieved properly.

I. INTRODUCTION

Even if the operation of a motor drive on mains with constant frequency depicts the majority of industrial usage, drives at variable supply frequency also have a dedicated area of application. For reliability reasons on the generating side the distribution of electrical energy on board of an aircraft is often realized by a network operating in the solitary operation at inherently variable frequency. Thus, an electrical device connected to this network is supplied by a frequency that corresponds to the current speed of the generator's turbine. The speed of the turbine is directly dependent on the aircraft's flight phase. Idling turbines would mean 360Hz network frequency at the minimum and the maximum value of the frequency is reached with 800Hz at aircraft's take-off. Applying the Dahlander winding [1] in this case would result in two speed ranges for electrical drives instead of two fixed speeds at constant supply frequency. For electrical drives with sophisticated speed control, power electronics is of course required to ensure the desired operating point at any rotational speed of the aircraft's main engines. If it succeeds to achieve the performance of a drive at two speed ranges, one may save the power electronic converter on the load side. This means to take advantage of the benefits mentioned above which are of high interest in aircraft applications in particular.

In the present case the electrical network of the new Airbus A380 is subjected. Although the feeding pumps for cooling liquids do not have ambitious requirements with respect to speed control they are designed as converter-fed induction machines. Therefore, the performance of the machine's design with Dahlander winding is assessed by the example of a pump drive. The considered pump device consists of two separate induction machines, each equipped with a pump fan wheel and working in parallel on a common liquid cooling circuit. As this exercise involves a prototype solution for an already existing system
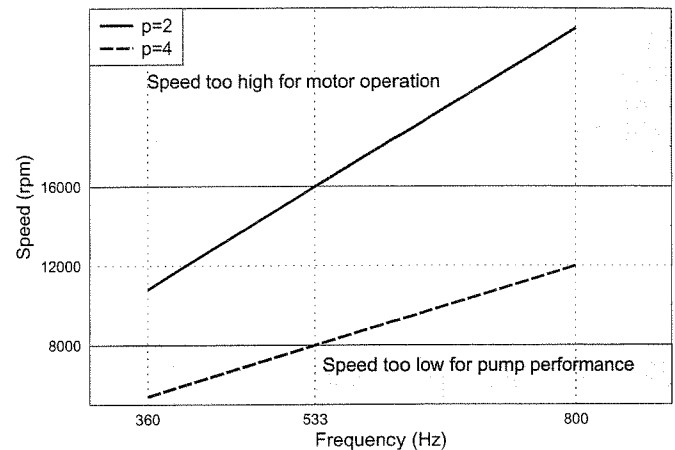

Figure 1: Speed Characteristics.

with installation constraints, stator diameter and rotor length are limited for the new motor design. To find an optimal solution for the motor design at these limiting constrains, finite element calculations are performed.

The mechanical output power of the motors are $P = 2\,\text{kW}$ each, the frequency range is $f = 360 - 800\,\text{Hz}$ and the range of the machines speed is $n = 8000 - 16000\,\text{rpm}$. Those requirements result in a stator design with pole pairs $p = 2$ and $p = 4$ of the Dahlander winding. The speed vs. frequency characteristics is shown in Fig. 1.

The principle of pole changing windings, and the special case of the Dahlander winding were developed at the end of the 19th century. A comprehensive overview of pole-changing windings is given in [1] and [2]. In the 1950s and 60s, the principles were generalizes and the techniques were improved. The pole-amplitude modulation (PAM) and the pole-phase modulation (PPM) were developed as such generalized pole-changing techniques [3], [4]. In their theory, the PPM is considered the most general winding design approach, of which the PAM is a specialization, and again, of which the Dahlander winding is a specialization. Each specialization limits the choice of the pole ratio p_1/p_2. For example, the Dahlander winding is only capable of generating fields of pole ratio 2:1, a PAM winding however can generate pole ratios of $n : (n - 1)$ with n as an integer. In addition to the improvements, which were achieved in the development of the winding, the pole-changing winding gained new fields of application with upcoming power electronic devices. In the 1990s pole-changing techniques were used together with an inverter supplied induction motor to extend the speed range for traction applications [5], [6]. These approaches represent variable-frequency pole-changing techniques, however, they cannot be compared to the approach of this paper, since the technical problems differ, and the inverter is the component, which is eliminated using the approach proposed here.

In this paper the development of the induction machine is de-

picted comprehensively, starting with the basic analytical layout of the stator's cross-sectional geometry and the stator coils in particular. Due to the design constrains, the available stator space is to be used most effectively. Therefore, FEM calculations, one at each number of pole-pairs, are used to determine the optimum partitioning of the available stator space into copper and iron and between stator yoke height and teeth width.

The optimum design is chosen and manufactured. Finally, the performance of the prototype is assessed on an aircraft-system integration-bench and measurements are presented. Steady state measurements show that for the depicted pump drive, induction machines with Dahlander winding basically reach similar performance than the speed-controlled motors. Slight deviations are due to the imposed design constraints. Transient measurements show that the occurring current peaks do not exceed the values of the regular startup currents.

II. WINDING DESIGN ASPECTS

A. Analytical

General Design Procedure

The electromagnetic design procedure of an induction machine can be divided into the following steps [7]:

1. Determination of the main dimensions

2. Design of the stator winding

3. Design of the rotor winding

4. Design of the magnetic circuit

5. Verification of the design by means of field calculation

Typically, steps 1. to 4. are performed analytically. Step 5. however, can either be done also by analytical computation, or be means of numerical simulation, such as the finite element method. Especially, if the application requires for very high accuracy, numerical techniques are inevitable.

Based on the required characteristics rated power P_r, no-load speed n_0, rated frequency f_r, rated voltage V_r and number of phases m, the main dimensions, such as inside diameter of stator D as well as the length of the sheet stack l are determined.

The design of the stator winding is based on an assumed value for the mean airgap flux density B_m. The airgap flux is determined by,

$$\Phi_\delta = B_m \cdot \tau_p \cdot l , \tag{1}$$

where $\tau_p = \frac{\pi D}{2p}$ is the pole-pitch. For the design process, the airgap flux and main machine flux Φ_m are assumed to be equal and the number of winding turns is determined as follows:

$$w_s = \frac{\sqrt{2} \cdot V_h}{2\pi f_r \cdot \xi \cdot \Phi_m} , \tag{2}$$

where f is the supply frequency and V_h is the voltage induced by the main flux. This number of winding turns has to be realized by a parallel armature conductors, in N_s stator slots, and yields a total of

$$z_s = \frac{2 \cdot a \cdot m \cdot w_s}{N_s} , \tag{3}$$

conductors per stator slot. The number of slots per pole and phase q is used to calculate the winding factor ξ. Assuming the value of the rated power factor $\cos\varphi_r$, and considering the maximal admissible current density in the stator winding J_s, the value

of the rated stator current $I_{s,r}$ as well as the copper cross-section per conductor $A_{s,cu}$ is determined. From a given copper space factor k_{cu} the stator-slot cross-section is calculated:

$$A_{s,slot} = \frac{z_s \cdot A_{s,cu}}{k_{cu}} . \tag{4}$$

The maximum airgap flux density is assumed to be α_p times its mean value. Therefore, the minimum tooth width is calculated:

$$b_{t,min} = \frac{\alpha_p \cdot B_m}{B_{s,t}} \cdot \tau_{s,slot} , \tag{5}$$

for saturation to be limited and the maximum flux density in the stator tooth not to exceed $B_{s,t}$, where $\tau_{s,slot} = \frac{\pi D}{N_s}$ is the stator-slot pitch.

The design of the squirrel-cage rotor comprehends the choice of rotor-bar material, number of rotor slots and the determination of slot geometry. The number of rotor slots should be selected carefully to reduce time and space harmonics in the total airgap field, leading to low torque ripple and vibrational force excitation. The cross-section of the rotor bars is determined by

$$A_{r,slot} = z_s A_{s,cu} \cdot \cos\varphi_r \cdot \frac{J_s}{J_r} , \tag{6}$$

where J_r is the current density in the rotor bar and $cos\varphi_r$ is the rated power factor. The minimum tooth width is determined analog to (5).

For induction machines, the design of the magnetic circuit corresponds to the determination of the airgap width and the thickness of stator and rotor yoke. The airgap width depends on the bearings and is calculated by:

$$\delta = 0.25 \text{ mm} \cdot \sqrt[4]{P_{mech}/\text{kW}} , \tag{7}$$

where P_{mech} is the mechanical power of the motor. The minimum thickness of stator yoke is determined by

$$h_{y,min} = \frac{B_m \cdot \tau_p}{2 \cdot B_{s,y}} , \tag{8}$$

with $B_{s,y}$ being the maximum flux density in the stator yoke. The thickness of the rotor yoke is determined, analogously. It has to be verified that the tooth widths and the thicknesses of the yokes meet the requirements of the copper cross-sectional area.

The final step in the design process is the verification of the design by means of field computation. This can either be done using analytical or numerical methods. If the field computation does not confirm the initial design, the procedure described above has to be repeated. If additional design constrains apply, it may be necessary to find an optimal solution, which is closest to the requirements.

The design procedure described so far has to be altered for the design of induction machines with pole-changing winding. For these machines, two different number of pole-pairs p result from either two different no-load speeds or from two different rated frequencies, where the latter is to be discussed in this paper. In this case, the procedure above has to be performed twice, once for each number of pole-pairs. Starting with (1), it can be seen that the flux for the lower number of pole-pairs is twice the flux for the higher number of pole-pairs. To determine the number of winding turns, it is necessary to know how the induced voltage V_h depends on p. This relation however depends on the type of connection of the winding.

Table 1: Connection type and ratio of airgap flux densities.

B_{p_2}/B_{p_1}	p_2 is Y	p_2 is YY	p_2 is Δ	p_2 is $\Delta\Delta$
p_1 is Y	0.80	1.60	1.39	2.77
p_1 is YY	0.40	0.80	0.69	1.39
p_1 is Δ	0.46	0.92	0.80	1.6
p_1 is $\Delta\Delta$	0.23	0.46	0.40	0.80

Table 2: Rated parameters.

	$2p_1 = 4$	$2p_2 = 8$
Rated power P_r	2 kW	2 kW
synchronous speed n_0	12000 rpm	12000 rpm
Rated voltage V_r	115 V	115 V
Rated frequency f_r	400 Hz	800 Hz
Number of phases m	3	3

The Dahlander winding is constructed by separating the winding into two or more coils, which are reconnected. This reconnection can be in series, or in parallel. The type of connection being used can be a Y-connection, or a Δ-connection. For each combination, the ratio of airgap flux density can be computed as follows:

$$\frac{B_{p_2}}{B_{p_1}} = \frac{\xi_{p_1} \cdot w_{p_1} \cdot V_{h,p_2} \cdot p_2 \cdot f_{p_1}}{\xi_{p_2} \cdot w_{p_2} \cdot V_{h,p_1} \cdot p_1 \cdot f_{p_2}}, \tag{9}$$

where the voltage ratio results from Y- or Δ-connection and the turn ratio from the series or parallel connection. Note, that (9) includes the ratio of the supply frequencies. For the commonly used case of constant frequency, this term cancels out. In the case of constant speed, variable frequency, the frequency is inversely proportional to p, thus (9) simplifies to

$$\frac{B_{p_2}}{B_{p_1}} = \frac{\xi_{p_1} \cdot w_{p_1} \cdot V_{h,p_2}}{\xi_{p_2} \cdot w_{p_2} \cdot V_{h,p_1}}. \tag{10}$$

Table 1 shows the ratios of the airgap flux density for various types of connection.

In [1], it is shown that the ratio of the winding factors $\frac{\xi_{p_1}}{\xi_{p_2}}$ is equal to 0.789 for $q_{p_1} = 2$ and approaches 0.816 for $q_{p_1} \rightarrow \infty$. Table 1 is exemplarily based on $\frac{\xi_{p_1}}{\xi_{p_2}} = 0.8$. The choice of the ratio B_{p_2}/B_{p_1} depends on the application. Choosing this ratio close to unity, for example, leads to constant torque at two different numbers of pole-pairs.

If the type of connection has been chosen, the design process follows the steps 1) to 4) of the standard induction machine, however, the design is done for each number of pole-pairs individually. From (2) two different z_s are obtained, though one value for z_s has to be chosen to be implemented in the designed machine. The minimum value of the yoke height $h_{y,min}$ from (8) is typically larger for the lower number of pole-pairs. The cross-section of the rotor bars is determined according to (6) after the stator winding has been designed. Equations (5) and (8) have to be regarded, respectively.

Example

Now, the design process is applied to a cooling-pump induction motor under additional design constrains. The first requirement is not to exceed a certain outer stator diameter, and the second is to reuse an existing rotor design.

The rated parameters of the machine are given in Table 2. Since rated power and synchronous speed of both p are equal, torque of both p has to be equal, as well. Therefore, the ratio of the airgap flux densities for both cases is to be chosen close to unity. According to Table 1, a Δ-connection is chosen for $2p_1 = 4$ and for $2p_2 = 8$ a YY-connection is chosen. Due to the small size of the machine, the least possible number of slots is selected:
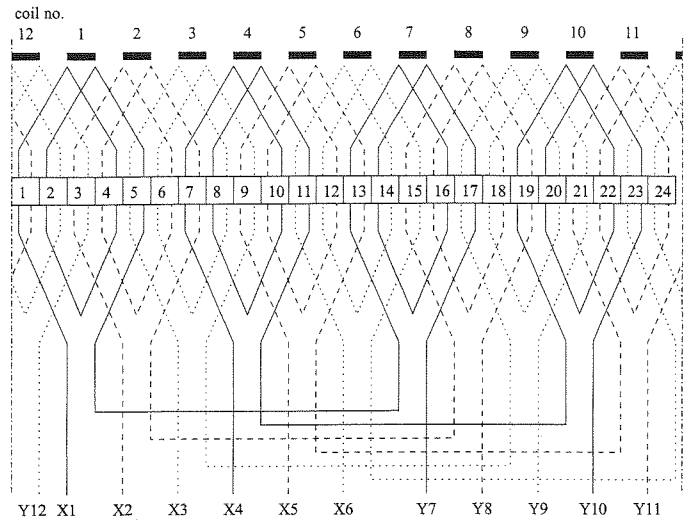
$$N_1 = m \cdot 2p = 3 \cdot 8 = 24. \tag{11}$$

Figure 2: Winding diagram.

This yields $q_{p_1} = 2$ and $q_{p_2} = 1$. The winding diagram is shown in Fig. 2 and the circuit diagram can be seen in Fig. 3. Switching from one p to another is done by connecting all lines of the Δ-connection to the star point of the YY-connection. In this way, coils 1,7 and 4,10 are brought together in the upper branch of the YY-connection.

According to (10), the ratio of airgap flux densities is calculated for the selected type of connection:

$$\frac{B_{p_2}}{B_{p_1}} = \frac{0.683}{0.866} \cdot \frac{2}{1} \cdot \frac{115\,\text{V}/\sqrt{3}}{115\,\text{V}} = 0.9107. \tag{12}$$

From (1) to (3), the airgap flux Φ_δ, the number of winding turns w_s and the number of conductors per slot z_s is calculated. Taken the Δ/YY-connection into account,

$$z_{s,p_1} = 38 \quad \text{and} \quad z_{s,p_2} = 35 \tag{13}$$

are obtained. To be sure to choose the main inductance of the machine sufficiently large for both p, $z_s = 38$ is selected. From
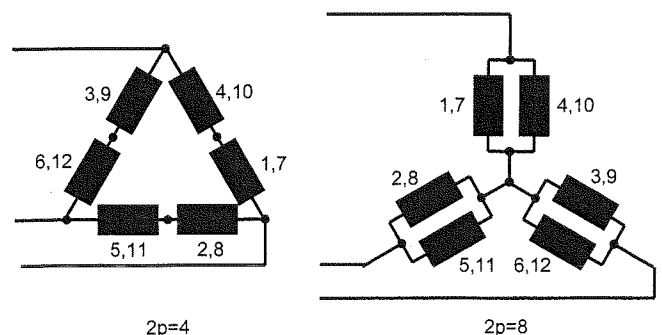

Figure 3: Circuit diagram.

assumed values for the rated power efficiency $\eta_r = 70\%$ and the rated power factor $\cos\varphi_r = 0.7$, rated stator current is computed. Using (4) the stator-slot cross-sectional required area is calculated

$$A_{s,slot} = 112.4 \text{ mm}^2 . \qquad (14)$$

Following the design procedure, the minimum width of the stator tooth and the minimum height of the stator yoke are computed according to (5) and (8), respectively:

$$b_{t,min} = 1.81 \text{ mm}, \qquad (15)$$

$$h_{y,min,p_1} = 3.63 \text{ mm} \quad \text{and} \quad h_{y,min,p_2} = 1.82 \text{ mm}. \qquad (16)$$

The provided slot cross-section area calculated from the fixed outer stator diameter $D = 80$mm and $h_{y,min} = h_{y,min,1}$ yields:

$$A_{s,slot}^* = 88.73 \text{ mm}^2 . \qquad (17)$$

The comparison of (14) and (17) shows that the requirement for the slot cross-section area cannot be fulfilled under the diameter design constraint. Increasing the dimensions b_t and h_y increases the overall magnetic reluctivity, however, the slot cross-section, and therefore the area, which can be used for the winding is reduced. This tradeoff becomes an additional aspect, which will be discussed in more detail in the next section.

B. Computations and optimization by means of FE models

As it can be seen from (14) and (17), the analytical design procedure does not yield a consistent design that fulfills all requirements including the geometrical design constrains. Therefore, the FEM is used to obtain the best performing solution under the geometrical constrains.

The two different number of pole-pairs generate conflicting demands on the usage of the available stator area. Where for the smaller number of pole-pairs an increase of the yoke height is most effective to increase the mean airgap flux density, for the higher number of pole-pairs the available area can be used more effectively as copper cross-section area. Another parameter, which may be varied, is the tooth width.

To find the optimal solution for this problem the FEM is applied. Therefore, a FE model is constructed with variable tooth width and yoke height as input parameter. In the given application of a prototype solution the rotor is neither known nor could the exact rotor geometry by determined bu non-destructive measurement. Therefore, the rotor is to be considered unknown and can not be modeled in detail. By counting the number of apparent rotor slots, the Carter factor of the rotor is estimated and the rotor is modeled as a solid cylinder, where the airgap width is increased by the estimated Carter factor.

For each combination of h_y and b_t, a two-dimensional finite element model is constructed [8], [6] and [9]. Since the exact geometry of the rotor slots of the induction machine is not known, the optimization can only be carried out with respect to the no-load condition and with respect to the mean airgap flux density. Therefore, it is sufficient to perform one static simulation of one time instance for each number of pole-pairs.

To avoid thermal overload, the maximum admissible current density has to be considered. Hence, the stator winding is excited by a current density, of which the rms value is equal to the maximum admissible current density in the winding.

In this case however, the voltage equation of the stator and the expected ratio of the airgap flux densities at constant voltage is not considered in the simulation. Therefore, the simulation
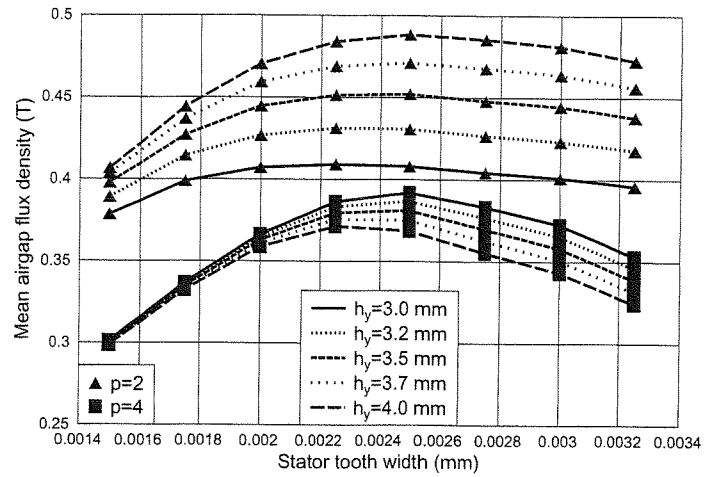

Figure 4: FEM simulation result: Mean airgap flux densities (for $p = 4$: calculated using (12)).

results of the second number of pole-pairs have to be multiplied by the expected ratio $\frac{B_{p_2}}{B_{p_1}}$.

For the induction motor presented in this paper, the simulation procedure described above is performed and the resulting mean airgap flux densities as a function of tooth width and yoke height are shown in Fig. 4 for $J = 6$ A/mm^2. It can be seen that for

$$b_t = 2.5 \text{ mm} \quad \text{and} \quad h_y = 3 \text{ mm} \qquad (18)$$

the mean airgap flux densities for both p are approximately equal to 0.4 T. It can be further seen, that $p = 2$ approaches this value from top to bottom, where $p = 4$ approaches it from bottom to top. Therefore, the optimization procedure can be stopped at $h_y = 3$ mm.

Since this is optimum combination of h_y and b_t for the presented machine under the given design constrains, it is chosen and the prototype is manufactured according to this design. The comparatively low value of the mean airgap flux density is due to the limiting design constraints.

The flux density distribution for $p = 2$ and $p = 4$ excitation are shown in Fig. 5 and 6, respectively. The plots clearly show the four pole and eight pole flux distribution. In addition, it can be seen that in the $p = 4$ case the maximum flux density is occurring in the stator teeth, where in the $p = 2$ case the yoke is saturating. This confirms the statement of different demand on the stator cross-sectional area.

In addition to the optimization by means of two static FE simulation per combination of yoke height and tooth width, there is an alternative, which may produce more accurate results at significant higher computational cost. This is to perform a static simulation for the one number of pole-pairs and calculate the flux linkage from integration of the magnetic vector potential. In stead of performing a second static analysis, the number of winding turns is calculated from the first simulation and the nominal voltage. This is then used to perform the second simulation as a transient voltage driven simulation , . This simulation, however, requires significant more computational cost.

III. EXPERIMENTAL RESULTS

A. Steady State

For performance verification two prototypes of the induction motor are manufactured according to the optimum design. Fig. 7 shows the stator together with the Dahlander winding. In Fig.
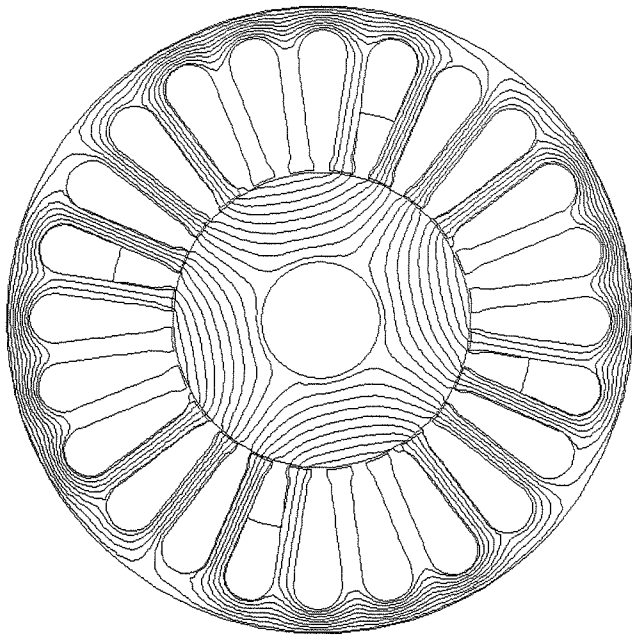
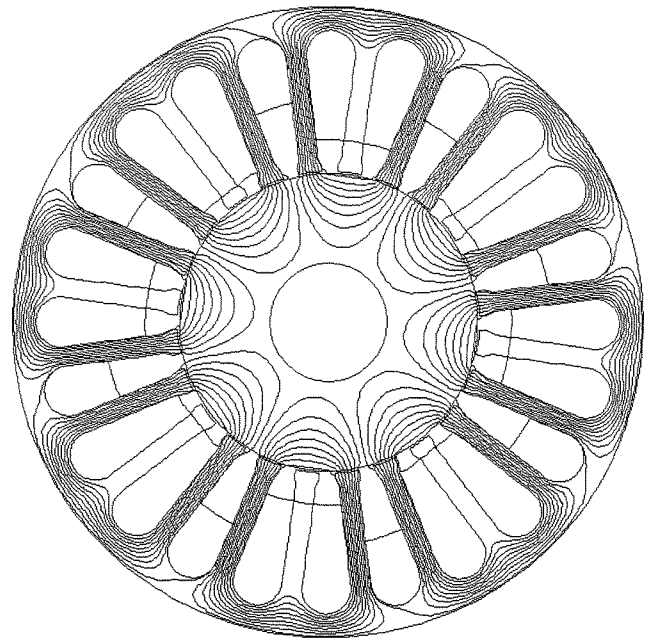Figure 5: Simulated flux density distribution for $p = 2$.

Figure 6: Simulated flux density distribution for $p = 4$.

8, the assembly of two machines in the pump housing are shown. It can be seen that the stator diameter is at its maximum values for the given pump construction.

The pump assembly driven by the two machine's prototypes is installed on the integration rig of the cooling system. This test bench depicts the full-size representation of the cooling system as it is installed on the aircraft, allowing overall system verification as an integral part of the design process. The pump assembly is working on the cooling circuit where it replaces the converter supplied one that is installed in standard configuration. The machines are connected to an appropriate contactor circuit that serves for switching the number of pole-pairs during operation. This device is connected to a power supply unit that allows free demand of input voltage and frequency. In the given layout two motors are installed on one pump assembly. Both motors drive a pump wheel each and are working in parallel on one cooling circuit. This is done for reasons of redundancy and not for increasing the flow rate. Therefore considering single pump operation is sufficient for the measurements.

The presented results are obtained at stator voltage $V = 115$ V and startup with $p = 2$ for stator frequencies in the range of $f = 360 - 500$ Hz. Each operating point characterized by the supply frequency is adjusted by the power supply unit's settings. When the speed of the machine reaches its limit at $n = 16000$ rpm the number of pole-pairs is switched to $p = 4$ and the frequency range $f = 450 - 800$ Hz is considered. A small overlapping range is taken into account for determining the most appropriate frequency for switching the number of pole-pairs.

Fig. 9 shows the measured flow rate of the cooling liquid in dependency on the supply frequency. For $V = 115$ V the flow characteristic is increasing continuously for both numbers of pole-pairs, $p = 2$ and $p = 4$ but is finally sloping down starting at a frequency of $f = 400$ Hz for $p = 2$ and 650 Hz for $p = 4$. As this behavior indicates a low voltage reserve further tests are performed at an increased supply voltage of $V = 200$ V. For stator frequencies belonging to the increasing branch of the flow characteristic, a higher supply voltage is not leading to an increased flow-rate as it is depicted in Fig. 9. In case that the flow characteristic is sloping for $V = 115$ V an increased supply
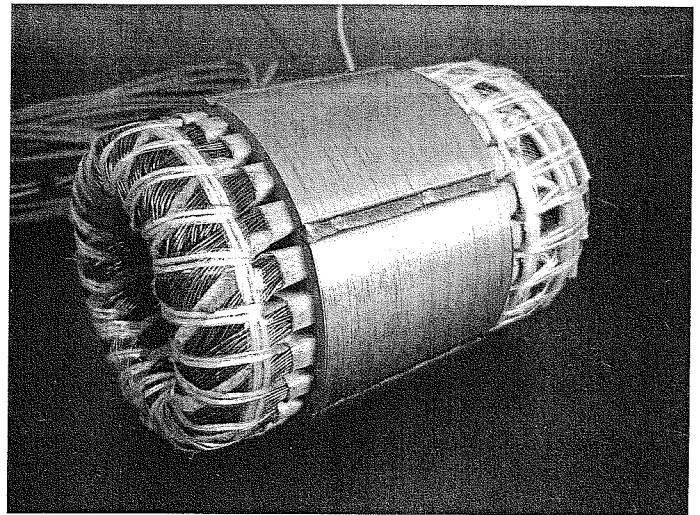

Figure 7: Stator with Dahlander winding.

voltage induces a significant increase in the flow-rate.

Before interpreting this behavior the typical torque-speed characteristic of an induction machine operated on terminals with constant voltage and constant frequency has to be considered. For the performed measurements it has to be emphasized that the pump drive is operated on separate characteristics, one for each frequency. Following the pullout torque is decreasing at increasing supply frequencies.

On the rising branch of the flow characteristic each operating point of the induction machine is determined according to the load torque that is given by the mechanical resistance of the liquid in the ducts of the cooling circuit. For those situations the pullout torque is higher than the load torque. Increasing the supply frequency at unchanged input voltage implies operating the induction machine on a different characteristic with a lower pullout torque. At a certain frequency pullout torque as the maximum torque is lower than the required load torque, therefore the flow is decreasing. Applying a higher stator voltage in this situation results in an immediate increase of the pullout torque and a stable operating point is set according to the load torque.
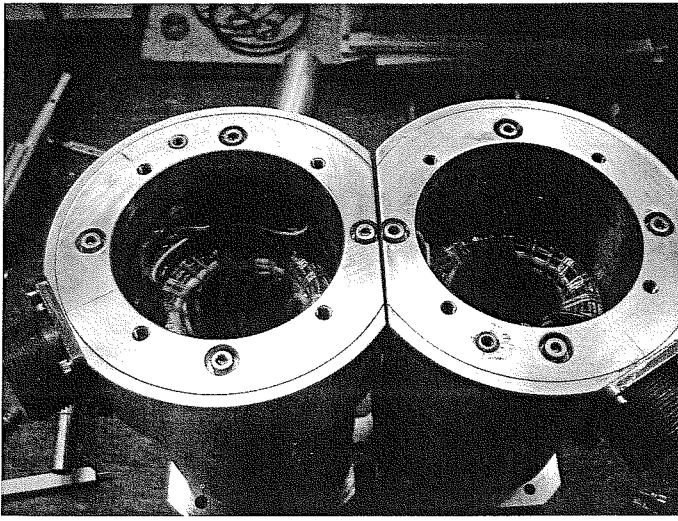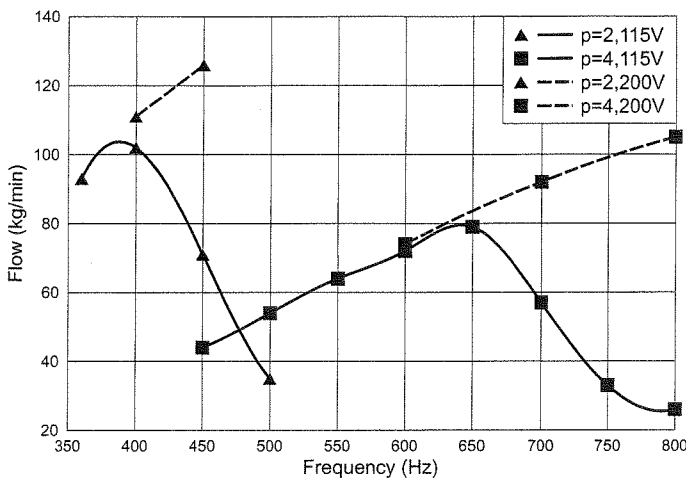
Figure 8: Two motors in housing.

Figure 9: Measured pump performance.

Figure 10: Measured current waveform, transition form p=2 to p=4.

Figure 11: Measured settling time.

Looking at the presented test results the following facts are revealed:

1. The maximum flow rate obtained with the Dahlander-wound machine prototype could be determined by experiment. This is according to the requirements of the cooling system and is shown as dashed line in Fig. 9.

2. The layout voltage of $V = 115$ V is obviously too low for covering the complete frequency range with a sufficient performance.

The deficiencies of the prototype design are related to the constraints of retaining an existing rotor and of limiting the stator diameter. With a fixed active length the machine's torque is restricted and a limited stator diameter results in iron saturation at low flux density and therefore in a low inductance of the machine.

Hence, the general applicability proof of the Dahlander-wound induction machine is successfully verified for the present application although a further optimization cycle has to be done.

B. Transient

In addition to steady state measurements (Fig. 9), the current waveforms during the switching process for both transitions, from the lower to the higher number of pole-pairs and vice-versa,
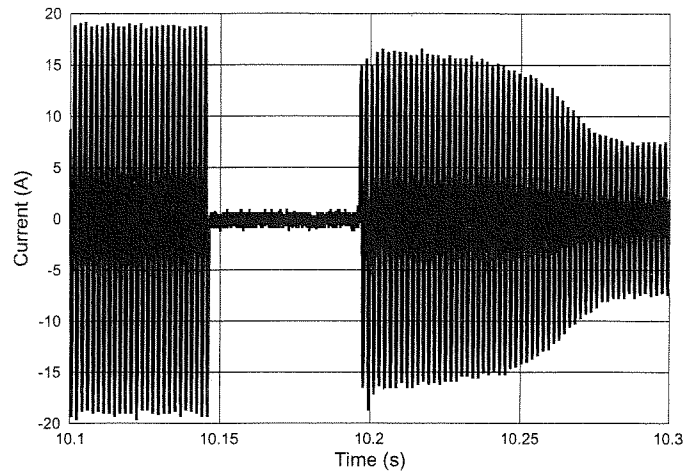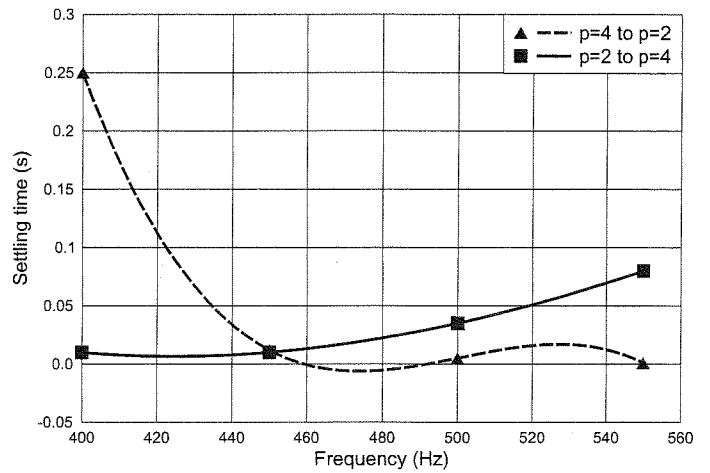
were measured. The measured current waveform for the transition from $p = 2$ to $p = 4$ at 115V and 550Hz is shown in Fig. 10.

The exact current waveform depends on the following parameters: frequency, stator voltage, and phase angle at switching time. Frequency and voltage indicate an operational point, of which the characteristics are: saturation/main inductance and slip/load. The phase angle at switching instant influences the magnitude of the current peak after switch-on. The settling time and the largest occurring magnitude of the current peak are shown in Fig. 11 and 12, respectively.

It can be seen, that in the interval, in which the switching is supposed to be performed, the current peaks and the steady state currents do not differ by much. Though a more detailed transient analysis, including the measurement of the stator-voltage in magnitude and phase, would reveal more insight into the switching process itself. It can be concluded, that the occurring transient current do not exceed the regular level of startup currents of the induction motors.

IV. SUMMARY AND CONCLUSIONS

In this paper, the design of a Dahlander-wound induction machine for operation on mains with variable frequency was presented. An initial design is obtained by analytical calculation. Due to the design constraints, an optimal solution, closest to the requirement need to found. Therefore, the FEM was used and
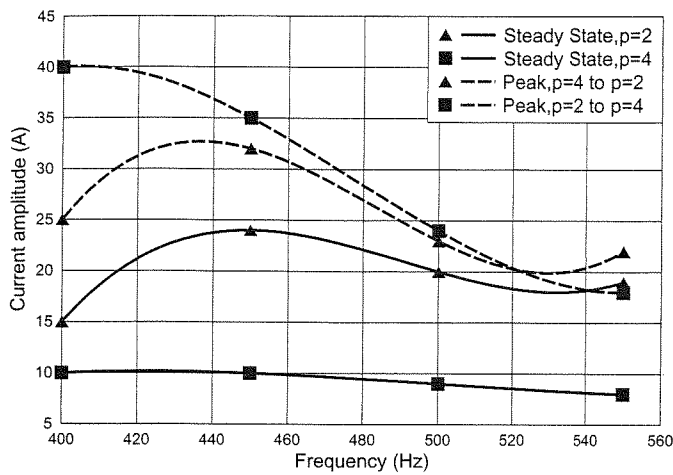
Figure 12: Measured current amplitude.

simulation procedure and results have been presented. The optimum design has been manufactured and put on a test bench. Steady state measurements show that the general performance of this approach meets the requirements that are given by a pump drive for an aircraft application. Replacing the motor that is usually operated on a power electronic converter, the presented layout offers an attractive solution for overall weight and cost saving and for increasing the reliability of the system. Measurements for transient operation show that current peaks after switching the pole-pairs are in an acceptable range. As the present design was limited by installation constraints, the performance has some short comings when the pump is operated at rated voltage. Therefore, further work has to be spent on the enhancement of the motor design.

V. REFERENCES

[1] H. Sequenz, *Die Wicklungen elektrischer Maschinen. Bd. 3. Wechselstrom-Sonderwicklungen.* Springer, 1954.

[2] H. Auinger, "Polumschaltbare Dreiphasenwicklung mit 6 Klemmen Übersicht zum Stand der Technik," *Bulletin des Schweizerischen Elektrotechnischen Vereins*, vol. 69, no. 17, pp. 926–932, 1978.

[3] ——, "Neuartige polumschaltbare Dreiphasenwicklung mit sechs Anschlussenden für elektrische Maschinen," *Siemens Forschungs- und Entwicklungsberichte*, vol. 7, no. 1, pp. 1–10, 1978.

[4] J. M. Miller, V. Stefanovic, V. Ostovic, and J. Kelly, "Design considerations for an automotive integrated starter-generator with pole-phase modulation," in *Industry Applications Conference, 2001. Thirty-Sixth IAS Annual Meeting. Conference Record of the 2001 IEEE*, vol. 4, 2001, pp. 2366–2373.

[5] M. Osama and T. A. Lipo, "A new inverter control scheme for induction motor drives requiring wide speed range," *Industry Applications, IEEE Transactions on*, vol. 32, no. 4, pp. 938–944, 1996.

[6] M. Mori, T. Mizuno, T. Ashikaga, and I. Matsuda, "A control method of an inverter-fed six-phase pole change induction motor for electric vehicles," in *Power Conversion Conference - Nagaoka 1997, Proceedings of the*, vol. 1, 1997, pp. 25–32.

[7] K. Vogt, *Berechnung elektrischer Maschinen.* Weinheim: VCH Verlagsgesellschaft mbH, 1996.

[8] A. B. J. Reece and T. W. Preston, *Finite Element Mathods in Electrical Power Engineering.* Oxford University Press, 2000.

[9] K. Hameyer, *Numerical Modelling and Design of Electrical Machines and Devices.* Southampton, Boston: WIT Press, 1999.

[10] D. Shen, G. Meunier, J. Coulomb, and J. Sabonnadiere, "Solution of magnetic fields and electrical circuits combined problems," *Magnetics, IEEE Transactions on*, vol. 21, no. 6, pp. 2288–2291, 1985.

[11] B. Brunelli, D. Casadei, U. Reggiani, and G. Serra, "Transient and steady-state behaviour of solid rotor induction machines," *Magnetics, IEEE Transactions on*, vol. 19, no. 6, pp. 2650–2654, 1983.

[12] H. de Gersem, R. Mertens, D. Lahaye, S. Vandewalle, and K. Hameyer, "Solution strategies for transient, field-circuit coupled systems," *Magnetics, IEEE Transactions on*, vol. 36, no. 4, pp. 1531–1534, 2000.

[13] H. De Gersem, R. Mertens, U. Pahner, and K. Hameyer, "A topological method used for field-circuit coupling," *Magnetics, IEEE Transactions on*, vol. 34, no. 5, pp. 3190–3193, 1998.

[14] P. Dular, C. Geuzaine, and W. Legros, "A natural method for coupling magnetodynamic h-formulations and circuit equations," *Magnetics, IEEE Transactions on*, vol. 35, no. 3, pp. 1626–1629, 1999.

[15] P. Dular, F. Henrotte, and W. Legros, "A general and natural method to define circuit relations associated with magnetic vector potential formulations," *Magnetics, IEEE Transactions on*, vol. 35, no. 3, pp. 1630–1633, 1999.

[16] M. Osama and T. A. Lipo, "Experimental and finite-element analysis of an electronic pole-change drive," *Industry Applications, IEEE Transactions on*, vol. 36, no. 6, pp. 1637–1644, 2000.

[17] H. Nam, S.-K. Jung, G.-H. Kang, J.-P. Hong, T.-U. Jung, and S.-M. Baek, "Design of pole-change single-phase induction motor for household appliances," *Industry Applications, IEEE Transactions on*, vol. 40, no. 3, pp. 780–788, 2004.

[18] K. C. Rajaraman, "Optimum designs of 1:2 pole-changing motor," *IEE Proceedings, Part B: Electric Power Applications*, vol. 129, no. 3, pp. 151–158, 1982.

AUTHORS NAME AND AFFILIATION

Michael van der Giet and Kay Hameyer
Institute of Electrical Machines
RWTH-Aachen University
Schinkelstrasse 4
D-52056 Aachen, Germany

Stephan Risse
Airbus Deutschland GmbH
Kreetslag 10
D-21129 Hamburg, Germany